J. Phys.: Condens. Matter **22** (2010) 055301 (15pp) doi:10.1088/0953-8984/22/5/055301

Degradation and rejuvenation studies of AC electroluminescent ZnS:Cu,Cl phosphors

Jacob Stanley, Yu Jiang, Frank Bridges, Sue A Carter and Laurel Ruhlen

Physics Department, University of California, Santa Cruz, CA 95064, USA

Received 29 September 2009, in final form 1 December 2009
Published 15 January 2010
Online at stacks.iop.org/JPhysCM/22/055301

Abstract

We report detailed degradation and rejuvenation studies of AC electroluminescence (EL) of the phosphor ZnS:Cu,Cl, aiming to better understand the physical mechanisms that control EL emission. We find that the AC EL emission spectra vary considerably with the AC driving frequency but all spectra can be fit to a sum of four Gaussians. During degradation, although there is a large overall decrease in amplitude, the *shape* of the emission spectra measured at a given AC frequency does not change. Annealing the samples after they are significantly degraded can rejuvenate the phosphors with a maximum rejuvenation occurring (for fixed annealing times) near 180 °C. Further, these test cells can be degraded and rejuvenated multiple times. However studies at slightly higher annealing temperatures (240 °C) show significant thermal degradation and, perhaps more importantly, a change in the spectral shape; this likely indicates that two distinct mechanisms are then operative. In extended x-ray absorption fine structure (EXAFS) experiments we find that the CuS nanoprecipitates in the ZnS host (∼75% of the Cu is in the CuS precipitates) do not change significantly after the 240 °C anneal; these experiments also provide a more detailed comparison of the local structure about Cu in pure CuS, and in ZnS:Cu,Cl. In addition, the EXAFS experiments also place an upper limit on the fraction of possible interstitial Cu sites, proposed as a blue emission center, at less than 10%. The combined experiments place strong constraints on the mechanisms for degradation and rejuvenation and suggest that EL degradation is most likely caused by either Cu or Cl diffusion under high E-fields, while thermal diffusion at slightly elevated temperatures without E-fields present, re-randomizes the (isolated) dopant distributions. Higher T anneals appear to damage the sharp tips on the precipitates.

(Some figures in this article are in colour only in the electronic version)

1. Introduction

Doped ZnS phosphors have been extensively studied [1, 2] since they were first prepared by Sidot in the mid-1800s [3], and are in use today. The ZnS:Cu systems, co-doped with other activators such as Cl, Br, Al, have the unusual property that they exhibit electroluminescence (EL) [4] using relatively low AC voltages, roughly two orders of magnitude smaller than is required for DC EL. The optical emission is assumed to be electron–hole recombination from electron and hole trap sites [1, 2]. A crucial feature of the ZnS:Cu phosphors is that Cu has a very low solubility in ZnS and forms conducting Cu_xS precipitates in the insulating ZnS host above Cu concentrations of order 400–500 ppm. These precipitates form as the crystal cools and transforms into the cubic sphalerite phase—the stable phase at room temperature [2, 5, 6] and the phase with the best EL [7]. Although some early papers assumed the defect was Cu_2S [8], we showed recently that at the nearest neighbor level, the main Cu_xS defect is close to that of CuS and quite different from Cu_2S [9]. Isolated Cu defects (∼400 ppm; either substitutional Cu_{Zn}, or possibly interstitial Cu_i [10, 11]) are believed to act as acceptor sites (hole trap), while Cl (Br, Al, etc) defects form shallow donor sites (electron traps) [1, 2].

Much of the early work was done in the '50s' and '60s' [8, 12], and in 1963 Fischer [8] reviewed the existing models for AC EL and discussed how consistent they were with

empirical data. Fischer concluded that only two options were viable for AC EL:—a model with bi-polar (holes and electrons) field emission from opposite ends of conducting needle-like CuS precipitates, and a similar impact ionization model which is a modification of Maeda's model [13]. The presently accepted model for explaining AC EL in such materials is the bi-polar field emission model that Fischer developed as an extension of earlier models [14, 8], It assumes that electron and hole trap sites exist close to the Cu_xS precipitates. Under AC excitation, equal numbers of electrons and holes are injected from sharp tips (via field emission) at opposite ends of the Cu_xS precipitates. Many of the charges are trapped on nearby hole or electron traps to form a polarization field that eventually opposes the field at the precipitate tips. When the field is reversed there is temporarily a very large field near the tips, which enhances field emission in the reverse direction, until a polarization field of the opposite sign develops. Each time the field is reversed, injected electrons can combine with trapped holes (from the previous half cycle) near the Cu_xS precipitate tips. Fischer notes that based on optical studies [7, 8], luminescence predominately occurs near the tip where electrons are injected into the ZnS host i.e. when the nearest external electrode is positive. However the nature of the precipitates is not well known—the size is small and the actual shape has not been imaged. Although ZnS is cubic at room temperature it is twinned and usually highly defective with many (111) deformation faults [6]. When etched with HCl, many etch pits are observed and a high density of planar stacking (111) faults is observed [6].

Since many studies indicate that Cl^- donor defects (or similar defects Br^-, I^-, Al^{3+} etc) are needed to have good AC EL, it is quite likely that the emission takes place from these shallow donor sites which localize the charge, rather than directly from the conduction band. Shallow donor (trap) states are known to exist just below the conduction band (CB)—0.3–0.8 eV below [8] for Cl^- (or Br^-, I^-, etc) while Suzuki and Shionoya [15] report a shallow donor band 0.1 eV below the CB for Al^{+3} co-activators. The main acceptor defects are believed to be isolated Cu on Zn sites (responsible for the green photoluminescence (PL)) and several aggregate defects, some involving Cu or pairs of Cu (proposed for the blue PL emission). The observed PL and AC EL emissions likely all start at one or more of the very shallow donor trap sites.

Another unusual feature of these phosphors is that under continuous AC excitation the EL decreases with time, but the degradation mechanism is poorly understood. Further the degradation occurs faster at elevated temperatures and is decreased for slightly reduced temperatures [16, 17]. We have recently observed significant rejuvenation of the emission from a ZnS:Cu,Cl phosphor under short anneals [9], and that provides a new probe of the dynamics in this system. Here we report our first detailed studies of this effect along with corresponding EL degradation studies. We show that most of the rejuvenation occurs on a short timescale (<1 h) and that the EL phosphors can be degraded and rejuvenated multiple times. We also explore the changing spectral shape with AC frequency and use the combined results to place stronger constraints on degradation mechanisms.

In addition, for anneals at slightly higher temperatures (240 °C), ZnS:Cu,Cl is significantly thermally degraded, and unlike the case for EL degradation, there is a significant change in the shape of the emission spectra for a given AC frequency; one possibility is that there may be changes in the CuS precipitates. To investigate local structure changes about Cu in the precipitates we use the extended x-ray absorption fine structure (EXAFS) technique to see if the precipitates change significantly—any break-up of the precipitates or a size decrease caused by Cu diffusion into the host. We also use EXAFS to look for evidence of interstitial Cu which has been proposed for one of the emission centers [10, 11]. About 25% (∼400 ppm) of the Cu is either substitutional (Zn site) or interstitial. For the latter, the local Zn neighbor distribution would be quite different from that around a substitutional site and can be observed in EXAFS.

Before presenting the new results we first provide more details about the emission centers and the models for AC EL in section 1.1.

1.1. Background—EL emission centers

The exact nature of the AC EL emission centers is poorly understood and much of the early literature appears to have been forgotten; an early review of the emission centers was given by Shionoya *et al* in 1964 [18]; more recent summaries are provided in 1999 by Shionoya [1] and Tanaka [2]. Note that the models for AC EL described briefly above [8, 13] do not depend on the specific emission centers—only that hole and electron trap sites exist and recombination of electrons and holes leads to luminescence. Several different emissions have been observed in ZnS when doped with various atoms, and a number of models proposed [1, 8, 18]. However most of these emission-center models are based on photoluminescence of the entire sample and may differ from the AC EL in which the electron/hole excitation is via electron and hole injection. In particular, the electron/hole injection occurs over a very tiny volume of the sample and the local electron and hole densities may be much higher than under photoluminescence.

Pure ZnS has a UV emission, but no visible luminescence [19, 8]. When Cl^- is substituted for S (but no Cu or other 'activator' dopants added) a blue line is observed near 440 nm (2.8 eV); the material is often referred to as 'self-activated' (SA). Since Cl has only one negative charge there must be compensating charge defects—e.g. two Cl^- on S sites, together with a Zn vacancy (they need not be on adjacent sites and several different configurations are possible). It is likely that the Zn vacancy is involved in the 2.8 eV blue emission and Shionoya *et al* [18] suggest it is a transition of an electron trapped on a Cl^- site to a Zn vacancy aggregate acceptor (this aggregate center [20] is composed of the Zn vacancy, a Cl^- and three neighboring S^{2-}; holes are trapped primarily [21] on the three S^{2-}). A few reports have also suggested that undoped ZnS gives the same blue emission as this SA center and it is also attributed to Zn vacancies.

When Cu atoms are substituted at the Zn sites (but no Cl dopants), there are two emission lines—a blue line very close to that for the SA center and a red line—'Cu–R' (670 nm, 1.81 eV). The intensity of the red line appears

to depend on how the sample is prepared [22]; since it is not observed in any of our AC EL data, we do not consider it further. In evaluating possible models for Cu in ZnS it is important to note that all ZnS samples (doped with Cl, Cu or a mixture of these atoms) are diamagnetic over a wide temperature range from 1.5–300 K. This result is based on detailed susceptibility measurements by Bowers [23]; the technique has very high sensitivity (a few ppm) and is sensitive to any unpaired electrons that have paramagnetic moments. This rules out a wide range of possible defects when the system is not excited, including Cu^{2+}, Cu^{0}, and even Zn^{1+} or S^{1-} defects, as all would be paramagnetic. The lack of an ESR signal in (unexcited) Cu-doped ZnS supports this finding [24]. Thus copper is Cu^{+} in all these samples when not excited, including samples with higher concentrations containing CuS precipitates. For a +Cu charge, there must also be other nearby defects for charge compensation—two Cu^{+} on Zn sites plus a S vacancy, or two adjacent Cu^{+} ions, one on a Zn site and one interstitial. Note that Cu^{+} has a d^{10} configuration with no empty d-states, and thus cannot take part in the blue emission. However, when a hole is trapped on a substitutional Cu^{+}, one of the d-states becomes vacant [25] and a temporary d^{9} configuration (Cu^{2+}) is formed. In cubic symmetry, these d-states are split into t_2 (upper) and e (lower) states, with a splitting (observed in the infra-red) about 0.75–0.95 eV [25, 15]. For lower symmetry aggregate defects such as substitutional Cu adjacent to S vacancies or to Cl on S sites, the Cu d-states can be split further. Suzuki and Shionoya [15] and also Apple and Prener [25] suggest that the highest t_2 state is about 1.3 eV above the valence band, at least for a Cu–Cl pair.

For the blue line, Cu–B, Blicks *et al* [10] proposed that the emission center is formed from an adjacent pair of Cu^{+} sites, one substitutional and one interstitial; Urabe *et al* [26] using polarized optical measurements, concluded that the blue line arose from a center that has either a C_{3v} symmetry (such as the association of a substitutional Cu^{+} with an interstitial [10] Cu^{+}) or is a more complex center. Note that there are three blue lines observed in the ZnS systems; a blue line for only Cl doping (the SA center), a blue line for only Cu doping (the Cu–B center) and a blue line when the sample is co-doped with Cu and Cl, but not equal concentrations. There are also small shifts reported. It is not clear if these are really the same line, slightly perturbed by other dopants, or actually distinct lines. Bol [11] has also discussed the uncertainties about the blue emission centers. For now we refer to these as aggregate Cu cluster emissions.

When Cl or other co-activators (Br, I, Al) are added together with Cu, often in comparable numbers, a green line near 520 nm (2.4 eV) is observed as well as the blue line; whether the emission is blue or green depends on the Cu concentration and the Cu/Cl ratio. The optimum Cu concentration for the blue line to be dominant is 0.065%, with a low Cl concentration, while for 0.01–0.04% Cu with comparable Cu and Cl concentrations, the green line is dominant [23, 18]. Note that when Cl^{-} substitutes for S, it compensates Cu^{+} on Zn sites. In subsequent polarized optical measurements, Suzuki and Shionoya [15] showed that

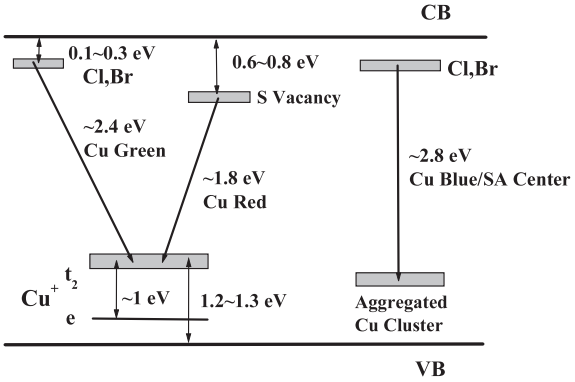

Figure 1. Some of the proposed energy levels within the band-gap of ZnS for various dopants and acceptors.

the green line—Cu–G—arises through a transition from a localized shallow donor state (assumed to be Cl^{-}) to a trapped hole on a Cu^{+} substitutional defect. Also Thornton carried out a detailed study of AC EL as a function of Cu and Cl concentrations [27]. He showed that the highest EL emission occurs for comparable concentrations of Cu and Cl and that the blue line occurs for lower Cu concentrations. Note that Cu atoms on Zn sites and the Zn vacancy complex (Zn vacancy, Cl^{-}, and three S^{2-}) both form acceptor sites which act as hole traps, while Cl^{-}, Br^{-} etc on the S sites or Al^{3+} on a Zn site form donors which trap electrons. A brief summary of some of the proposed defect energy levels are shown in figure 1.

Unfortunately the number of possible luminescence centers may be much larger than described above. Although doped ZnS (with Cu, Cl, Br, etc) is diamagnetic and hence has no ESR signal, UV excitation at low temperatures produces a range of meta-stable, paramagnetic states with very long lifetimes, and several authors [24, 28, 21, 29] have reported ESR signals after UV excitation. In particular, Holton *et al* [24] report at least seven distinct ESR signals associated with Cu, for samples prepared in different ways. The ESR technique probes the entire phosphor sample and not specifically the tiny regions adjacent to the CuS-like precipitates. However it is very sensitive and can detect very small concentrations of centers.

One aspect continues to remain poorly understood and has limited the use of these phosphor in many potential lighting applications. The problem is that under AC operation the EL luminescence decreases with time [2], whereas the photoluminescence, (from the rest of the bulk material) remains unchanged. Lehmann noted that this degradation (sometimes referred to as 'maintenance' [30]) is often best described in terms of the number of AC cycles applied to a cell [31]; the emission output decays at various rates, depending on the operation AC frequency. Lehmann [31] reports that for several standard ZnS:Cu,Cl phosphors the half-life (number of cycles to reduce the output by 50%) was typically between 10^{7} and 10^{8} cycles but in some cases could be increased to $\sim 10^{9}$ by air baking [30]. By substituting Br for Cl, i.e. ZnS:Cu,Br—Jaffe [32] obtained half-lives of 10^{9}–10^{10} cycles. These numbers are comparable to the lifetimes of commercially available ZnS:Cu phosphors today—lifetimes

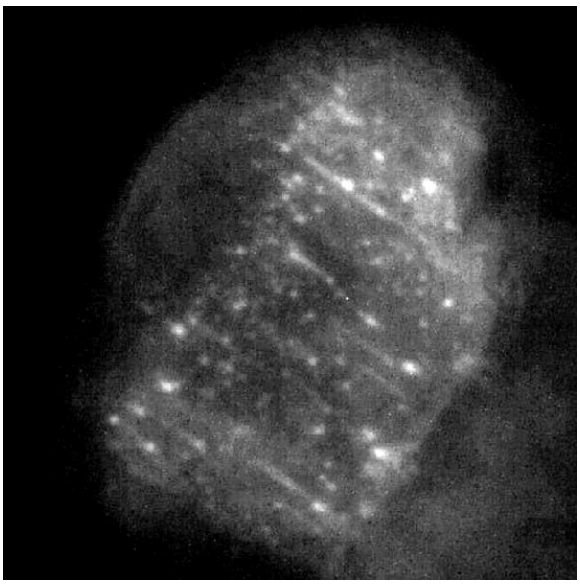

Figure 2. Microscope image of one of the 30 μm particles showing the bright spots of EL emission for 100 V square-wave at 100 kHz. Some spots appear as lines. Scale of picture 35 μm $\times$ 35 μm.

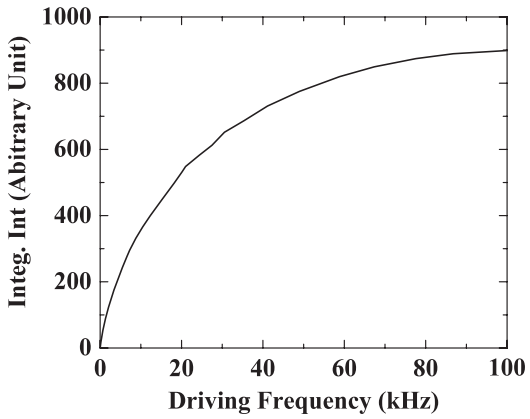

Figure 3. The change in integrated output as a function of AC frequency for a 100 V square-wave;—the curve is not linear over any of the frequency range and saturates just above 100 kHz.

of a few thousand hours when operated at 400–500 Hz. Thus there has been little improvement in the lifetime of these phosphors over the last three decades.

Although the actual degradation mechanism(s) are not known most agree that it probably involves some type of diffusive process, and several mechanisms have been discussed in the literature. Fischer [8] proposed that sharp tips on the CuS precipitates become damaged (blunted) under the large electric fields, leading to decreased electron/hole injection. However no further experiments supported this mechanism [29]. Other authors suggested that S vacancy diffusion is important; Lehmann [31] found that ZnS:Cu,Br (or similar (Zn,Cd)S phosphors) fired in pure sulfur have increased lifetimes. Jaffe [32] reported an increase in thermoluminescence at $-50\,^{\circ}$C for AC EL degraded samples which he attributed to increased S vacancies presumably near the CuS precipitates; however others have not been able to reproduce these results [29]. Hirabayashi *et al* noted (using several techniques) that the sulfur vacancy density did not increase after deterioration but that an increase in S vacancies is one of several factors that contribute to an accelerated EL deterioration [29]. Jaffe [32] found that after long EL degradation (600–1000 h at 4000 Hz) other defects formed that gave peaks near $30\,^{\circ}$C in the thermoluminescence spectrum. This indicates that deep trap sites with very long lifetimes can form, but since they do not occur until late in the degradation process, it is not clear that these centers are responsible for the main EL degradation. It is likely that other processes such as Cu or Br diffusion plays an important role [29].

To summarize, the EL emission decreases with time if: (1) the number of hole/electron trap sites decreases, (2) the efficiency of electron or hole injection decreases as a result of damage to the sharp tips of the CuS-like precipitates, (3) the emission centers are damaged, or (4) local damage to the ZnS (vacancies, interstitials, etc) changes the number of occupied trap sites or introduces deep trap sites. Damage might provide other de-excitation pathways for the trap sites, or form different types of electron and hole sites that do not as readily produce e–h recombination. Most of these possibilities have been mentioned but because of the complexity of this system, definitive experiments have not been found.

2. Electroluminescence experiments

2.1. Degradation and rejuvenation

As indicated above, although AC EL devices based on ZnS:Cu,Cl degrade significantly after operation for more than a day at 100 kHz and 100 V (200 V peak-to-peak), they can be significantly rejuvenated by a short anneal at modest temperatures [9]. Here we explore some of the details about the degradation and rejuvenation processes.

The test cells used for these experiments have the structure shown in the inset of figure 4(a). The 20–30 μm ZnS:Cu,Cl particles (DuPont) were mixed in an organic paste and spread in a thin layer about 25 μm thick, on top of a transparent P-DOT electrode, which was deposited on a thin glass plate. A thin layer of silver paste formed the second electrode. The cells were mounted in a light tight enclosure and connected via an optical fiber to an Ocean© digital spectrometer. AC EL spectra were collected from 350 nm $\rightarrow$ 700 nm for a variety of conditions. We also took microscope pictures of the 20–30 μm particles showing the tiny bright points of light emission believed to emanate from regions near the CuS-like precipitates; an example is shown in figure 2.

The integrated EL is known to increase with increasing AC frequency but saturates at high frequency. This occurs for all our test cells—see for example, figure 3. To investigate large degradations in a reasonable time-frame, some of the experiments were run at 100 kHz, but it is not clear how well one can extrapolate high frequency results to low frequencies. Consequently we include a few measurements at 1 and 5 kHz.

Several examples of the changes in the EL spectra during degradation are shown in figure 4. Figure 4(a) shows successive spectra for times ranging from 0 to 1200 min (20 h),

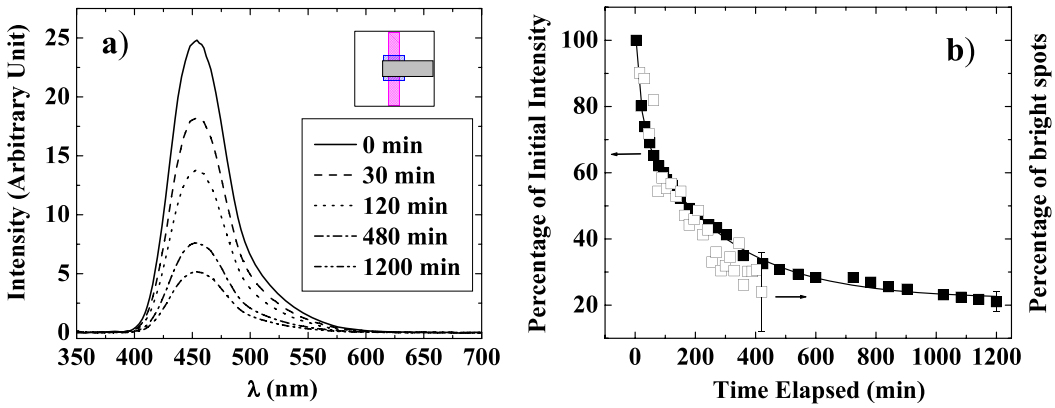

Figure 4. (a) Examples of the electroluminescence spectra at successive times of operation using a 100 V square-wave and 100 kHz. (b) The decrease in the integrated intensity of the spectra shown in (a) as a function of time (solid square). The decay can be fit to a sum of two exponentials plus a constant, (fit—solid line) (parameters: amplitudes A_1 and $A_2 = 31$ and 53, time constants t_1 and $t_2 = 17$ and 284 min.; constant = 22). For comparison, we also plot the percentage of bright spots in several 20–30 μm particles as a function of operating time (open square) in the same figure; using a two-exponential-fit as above, we get similar results, but with an uncertainty of 25%. A representative error bar for each data set is given in the last symbol.

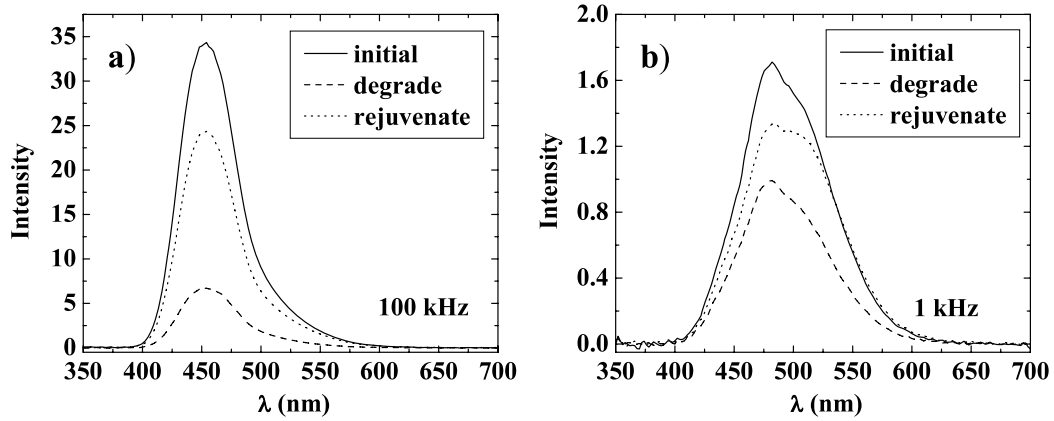

Figure 5. Examples of the change in the EL spectra between as-made, degraded, and rejuvenated via a 2 h anneal at 180 °C. (a) shows the spectra using a 100 V square-wave at 100 kHz—note no change in the shape of the spectra after degradation or after the anneal. (b) Similar data for operation (and degradation) at 1 kHz. The amplitude is much reduced and the shape of the spectra differs from that in part (a), but again does not change with degradation; however there is a small shape change after the anneal.

during the degradation using a 100 V square-wave at 100 kHz. Figure 4(b) shows the non-exponential decrease in intensity as a function of time over a 20 h period (100 V square-wave, 100 kHz) which can be fit to a sum of two exponentials plus a constant—see caption for parameters. We also noted that the number of bright points in a ZnS particle, such as in the microscope image shown in figure 2, decreases with time during operation. For comparison, we also plot (in figure 4(b)) the decrease in percentage of bright points observed in several 20–30 μm particles as a function of time for another similar device. The decay is similar to the decay of integrated intensity, but since this data set has a large error bar, the fit result has an uncertainty of ∼25%.

Figure 5 shows spectra for two other cells, one operated (and degraded) at 100 kHz and the other at 1 kHz. For each sample we plot the spectra for as-made, after degradation for 20 h, and after rejuvenation using a 2 h anneal at 180 °C. Panel (a) shows the spectra measured when using a 100 V square-wave at 100 kHz. Note that both during degradation or after the rejuvenation anneal, the shape of the spectra has not changed, it is *only an amplitude effect*—i.e. when normalized, the spectra overlap exactly. Panel (b) shows similar results when measured at a much lower frequency (100 V square-wave at 1 kHz). For low frequency operation such as 1 kHz, the overall intensity is much smaller, the percentage degradation after 20 h operation is much less than for 100 kHz, and the rejuvenated intensity (after a 2 h anneal) is closer to the original intensity; on an absolute scale the degradation and rejuvenation are small. However if one compares the amount of intensity rejuvenation to the intensity lost during degradation at a given AC frequency, this fraction is about 66 ± 2% for all frequencies. Also note that at 1 kHz, the shape of the spectra again does not change significantly during degradation.

In contrast, there is a small shape change during rejuvenation when measured at 1 kHz; after annealing at 180 °C, the green component near 510–520 nm is slightly increased relative to the blue line—see figure 5(b). Thus temperature effects can be different than EL degradation and

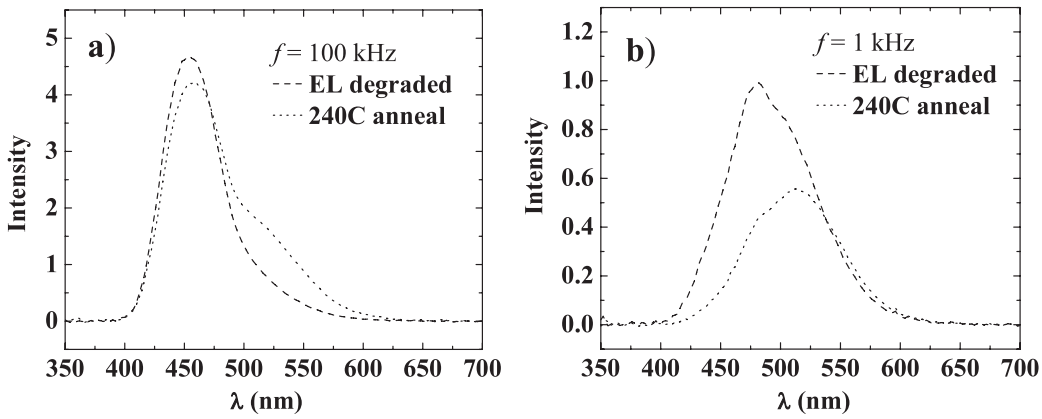

Figure 6. Comparison of the EL spectra for degraded samples (100 kHz operation, 100 V square-wave) and samples initially annealed at 240 °C, for 1 and 100 kHz operation. At 240 °C there is a significant change in the spectra shape that changes between 1 and 100 kHz.

the small shape change here for the rejuvenated sample is the first hint of this difference. To explore thermal effects further we compare in figure 6 the spectra for EL degraded samples with those for phosphor annealed at 240 °C before making a test cell. Again we use a 100 V square-wave at 1 or 100 kHz. Here large shape changes occur which differ for 1 and 100 kHz operation. These thermal anneal results show that in contrast to the EL degradation, there are significant changes in the spectral shape which must mean there is more than one type of emission complex. We return to a discussion of possible mechanisms in section 4.

To show in more detail the evolution of the line shape as the AC driving frequency varies, and also the lack of a significant change in shape of the spectra during degradation, we first normalized all spectra. In figure 7 we overlay the 'degraded' spectra (open circles) on top of the 'as-made' spectra (solid lines) for a few frequencies from 0.1 to 100 kHz. For a given AC frequency, deviations between spectra for the as-made and degraded samples are tiny for every frequency. However as the AC frequency is increased, the weight at shorter wavelength increases rapidly. The changes in peaks and shoulders as the AC frequency is increased, suggest that there are four separate lines, indicated by the vertical lines. Primarily it is the amplitude of each component that changes with AC frequency.

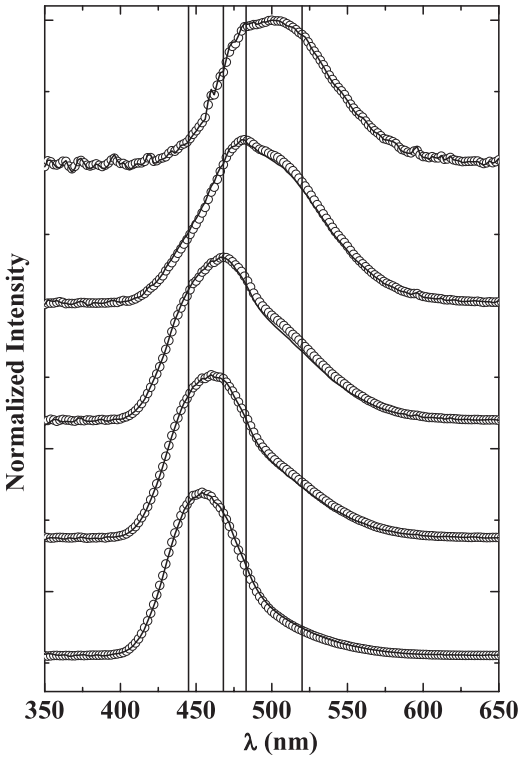

Figure 7. Comparison of normalized EL spectra for an as-made sample and after degradation at 100 kHz using a 100 V square-wave; the traces top to bottom are for AC frequencies 100 Hz, 1 kHz, 5 kHz, 10 kHz, 100 kHz. The solid line is for the as-made sample while the open circles are after degradation. There is a systematic shift to shorter wavelengths as the AC frequency increases, and a change in shape that suggests that all spectra are a sum of four spectral lines (indicated approximately by the vertical lines). Moreover, during degradation there is no significant change in the shape of the spectra for a given AC frequency.

2.2. Detailed rejuvenation experiments

For the first set of detailed annealing/rejuvenation experiments as a function of temperature, the test cells were EL degraded and annealed using the following procedures. The EL degradation was done by applying a 100 V square-wave at 100 kHz for 20 h. This reduced the luminosity of the device to ∼20% of its initial intensity. In order to explore the temperature dependence of annealing, many EL test cells were prepared and identically degraded as described above. Each cell was then annealed at a fixed temperature within the range from 130 °C → 240 °C. Ten cells were used to cover this range in roughly 10 °C steps. The initial, post-degraded, and post-annealed spectra were recorded for each cell and the integrated intensity calculated. To explore the AC frequency dependence two similar sets of experiments were carried out for 100 V square excitation at 5 and 1 kHz. Here the degradation times were also set to 20 h, although the amount of degradation is much smaller.

The results for these experiments are shown in figure 8 for operation at 1, 5, and 100 kHz (using 30 different cells; 10

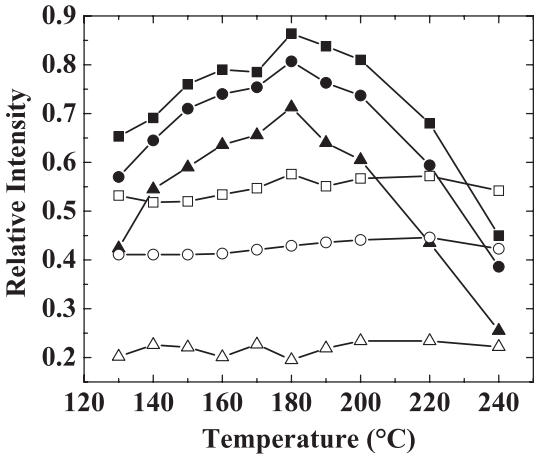

Figure 8. The relative intensity as a function of annealing temperature, following a 20 h degradation (100 V square-wave); frequencies 1, 5 and 100 kHz. Each set of measurements is made on a new device. The open symbols are for the degraded test cells while the solid symbols are after a 2 h anneal at temperature T following the degradation. Triangles—100 kHz; circles 5 kHz; squares 1 kHz.

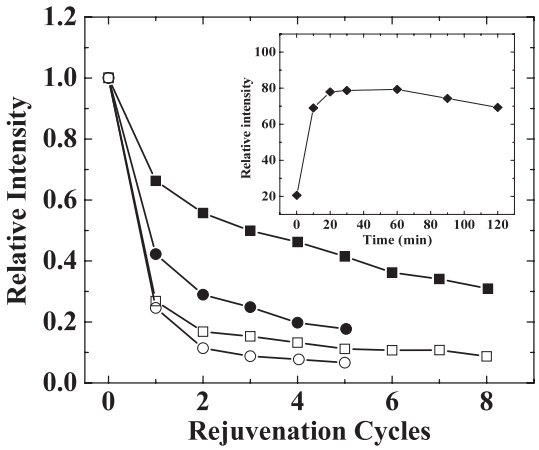

Figure 9. Changes in the rejuvenated output as a function of the number of repeated degradation–rejuvenation cycles for two different cells—one annealed at 180 °C (squares), the other at 220 °C (circles). The open symbols show the degraded intensity at each cycle, while the filled symbols give the rejuvenated intensity. At 220 °C the amount of rejuvenation is small by the 4–5th cycle, while for the optimum 180 °C annealing temperature, there is still a moderate rejuvenation after 8 cycles. Inset: shows the change in the EL emission versus the cumulative annealing time at 200 °C, after a 20 h degradation (100 V square-wave, 100 kHz). After each short anneal at 200 °C, the sample was cooled to room temperature, and the EL emission measured with a 100 V square-wave at 100 kHz. The x-axis is the cumulative annealing time.

cells for each frequency). The open symbols show the relative intensity after degradation, while the solid symbols show the intensity after a subsequent 2 h anneal at different temperatures (see figure 8 for details). Note that although the intensity varies from device to device (see for example figures 4 and 5) the relative intensity after a 20 h degradation for each device is reasonably constant at a given frequency. However the degree of rejuvenation varies substantially with temperature. Low temperatures below 130 °C produce little rejuvenation—the rejuvenation peaks near 180 °C and then decreases for higher T. In particular for anneals at 240 °C there is no significant rejuvenation. In our previous study [9] we obtained a slightly higher rejuvenation at 200 °C, roughly 91–92%, compared to ∼84% for the batch of EL material used in the current study; it is not clear why. However all the samples in the current study were prepared from the same materials in the same way and were repeatable to about 5%.

In addition, for the 240 °C anneal the binder is starting to degrade and begins to turn brown. Thus the lack of significant rejuvenation at 240 °C is partial due to binder degradation. In the experiment discussed earlier, in which we annealed some material at 240 °C *before* making a test cell—see figure 6, we found that along with the change in the shape of the optical spectra, there was also a 50% reduction in EL emission intensity. If instead, one starts with a new test cell, and then anneals the phosphor/binder mix 240 °C without any EL degradation, the emission is reduced to roughly 25%. Thus the emission after rejuvenation at 240 °C in figure 8 is probably too low, but the overall trend will not change. Similar experiments were carried out at 1 and 5 kHz frequencies—circles and squares in figure 8.

An obvious question is whether this degradation/rejuvenation cycle can be repeated many times. The answer is a limited yes; it can be repeated, but only a small number of times (6–8 cycles when annealed at 180 °C). We show the rejuvenation as a function of the number of degradation–rejuvenation cycles in figure 9 for two cells; one annealed at 180 °C and the other at 220 °C. For 180 °C some rejuvenation occurs even at the 8th cycle, while for 220 °C the rejuvenated intensity is small at the 4th–5th cycle.

After completing the above temperature study we briefly investigated the rate at which a device rejuvenated at 200 °C, during a series of successive short anneals, 10–30 min in length. After each short anneal the AC EL was briefly measured at the same frequency and voltage (100 kHz and 100 V) at room temperature. The integrated intensity is plotted in figure 9 inset as a function of cumulative annealing time. Most of the rejuvenation occurs in the first 15–20 min, with a peak rejuvenation near 1 h. For longer anneal times the EL emission begins to decrease slightly. Note that the net rejuvenation in this process is less than that from a single anneal for the same length of time, perhaps because of the additional operation at 100 V (100 kHz) or because repeated heating and cooling also changes the output.

2.3. Decomposition of EL spectra

In figure 7 we noted that all spectra appear to be a sum of four lines. To investigate this possibility further, we converted each spectra from a wavelength to an energy spectra (x-axis in eV) using the equation below, and normalized its height to 1.

$$S(E) = S(\lambda(E)) \times \left|\frac{\mathrm{d}\lambda(E)}{\mathrm{d}E}\right| = S(\lambda(E)) \times \frac{\lambda^2}{hc} \quad (1)$$

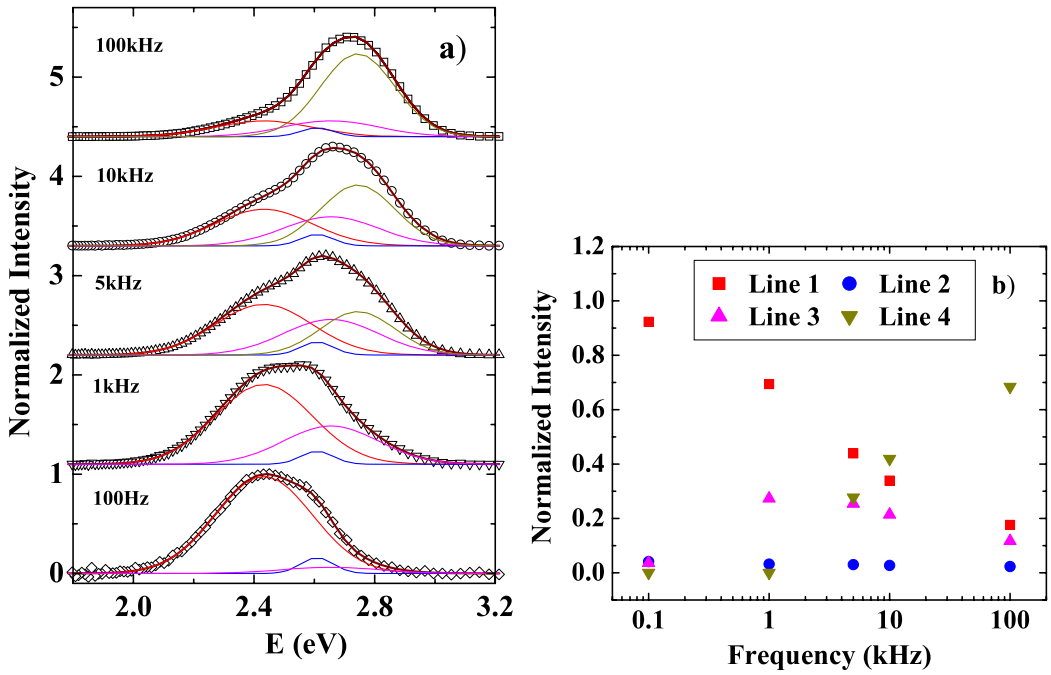

Figure 10. (a) Fits of the normalized AC EL spectra for 0.1, 1, 5, 10, and 100 kHz, showing four components, which are at the same position in each plot (table 1). The only variation as the AC frequency increases is a change in the relative amplitudes. (b) Plot of the relative integrated intensities (total area is normalized to 1.0) as a function of the AC frequency. See table 1 for positions and width of the lines.

Table 1. Positions and widths of the emission lines (in eV) from the fits to a set of Gaussian peaks for the spectra in figure 10(a). The uncertainty in the line positions is less than 0.03 eV for all lines and the uncertainty in the widths is less than 0.02 eV.

Line No.	Line position (eV)	Width (eV)
1	2.44	0.32
2	2.61	0.10
3	2.67	0.30
4	2.74	0.25

where $S(\lambda(E))$ represents a spectra in wavelength space, and $S(E)$ in energy space, here we use the energy–wavelength conversion equation, $E = \frac{hc}{\lambda} \approx \frac{1240(\text{eV nm})}{\lambda(\text{nm})}$.

Up to eight spectra were fit simultaneously, with the line position and width parameters common for all spectra (i.e. the widths and positions varied but were the same in every spectrum); only the amplitudes varied independently from one spectrum to the next. We find that *every* spectrum obtained for this material, including spectra obtained after a 240 °C anneal which degraded the phosphor (see figure 6), can be fit well with the same four spectral lines, with only a variation of the four amplitudes. The four line positions and half widths are given in table 1, and examples of the fits to normalized spectra for the as-made sample are shown in figure 10(a). The relatively large half widths obtained from these fits indicate that the lines are inhomogeneously broadened; the fluorescence lifetimes are long, of order μs and would lead to very narrow widths if the lines were homogeneously (lifetime) broadened. Note that line #2 is narrow, and although the integrated intensity is small it has observable amplitude over a narrow energy range; it is particularly needed to fit the spectra below 2 kHz.

In figure 10(b) we plot the relative amplitudes versus AC frequency to show the different behavior for the four lines (the changes for unnormalized spectra are very large and could not be compared on a linear plot). For this plot we have normalized the area under the curve to 1.0, so that the plotted amplitudes are the fraction of the area for each scan. Note that line 2 is different from the rest; it has a narrow line width, its integrated intensity is only a few per cent and it does not change much with AC frequency. However because of the small width it has appreciable amplitude over a narrow energy range and is needed for spectra at 1 kHz and below. Most of the intensity is in lines 1, 3 and 4. As the AC frequency increases the relative amplitude of the green line (#1) decreases, line #3 first increases and then decreases, while line #4 is negligibly small at low AC frequency but dominates at 100 kHz. In absolute terms with increasing frequency, first line # 1 saturates and then line #3 saturates; at 100 kHz line #4 is nearly saturated.

Finally we note that for thermal anneals, starting about 180 °C, and with the largest effects at 240 °C, the relative fraction (A_1/A_4) of the green line (2.44 eV) to the blue line (2.74 eV) increases with temperature, and for 100 kHz excitation, is nearly doubled at 240 °C. In these fits the line widths are the same as in table 1 within our errors; the line positions appear to move slightly to lower energy by 0.03 eV but that is also at the limit of our errors. A similar behavior is observed for the 240 °C annealed material when using 1 kHz EL excitation. Here the blue line has negligible amplitude; the main result is that the ratio of the amplitudes A_1/A_3 also increases with annealing temperature above 180 °C. A model for the above behavior is considered in section 4.

Ibanez *et al* [33] also investigated the frequency and voltage dependence of the EL spectra for a similar phosphor.

They fit the spectra using four Gaussian peaks and showed how these four Gaussian peaks change with AC frequency. However, our result differs from theirs. First, our spectra have a different shape when measured at a similar AC frequency—they find more weight in the long wavelength region and use a peak centered at ∼550 nm (2.25 eV). Second, their fit was done in wavelength space ([33] figure 5), while we want to explore the transition between various (broadened) energy levels and fit our data in energy space; most lines have different positions. Third, Ibanez *et al* found all their Gaussian peaks saturate near 20–30 kHz and have a 'similar saturation frequency', ([33] figure 6) while in our samples, the four Gaussian peaks saturate at quite different frequencies, and the shortest wavelength line saturates above 100 kHz. One other group has also fit the EL spectra to a sum of three Gaussians for 1 kHz excitation but they did not explore the frequency dependence or any degradation effects [34].

3. EXAFS experiment and data analysis

In section 2 we showed that above 180–200 °C, thermal anneals progressively changed the shape of the emission spectra, with the largest effect and a large red-shift at 240 °C (El experiments were not carried out for higher T). In addition, thermal anneals of the starting powder at 240 °C also degrade the EL emission. Further, other experiments show that the degradation occurs in a much shorter time as T increases [16, 17]—is this just increased diffusion or is there another mechanism at higher T? Therefore a major goal of the EXAFS study in this section is to check for non-thermal-phonon changes in the local distortions about Cu in the precipitates as T increases above 180–200 °C; such local distortions would indicate a change of the CuS precipitates. Possibilities include a break-up into smaller nanoparticles or dissociation of the CuS, with Cu diffusing into the ZnS host. Since the EL spectral changes increase rapidly with increasing T, we extended the temperature for the EXAFS to 550 K (277 °C) to maximize any effect. In addition we also use EXAFS to look for any evidence as to whether the proposed Cu interstitial sites for one of the blue emission centers, exists.

3.1. EXAFS experiment

Temperature dependent Cu K-edge EXAFS data were collected for ZnS:Cu,Cl materials at the Stanford Synchrotron Radiation Lightsource (SSRL) on beamline 10–2, using Si(111) monochromator crystals. Due to the low Cu concentration (≈0.1–0.2%) in ZnS:Cu,Cl, data were collected in fluorescence mode using a Ge multi-element detector. Zn K-edge data for ZnS:Cu,Cl and Cu K-edge data on a high purity CuS bulk powder were also collected in transmission mode to allow a detailed comparison between the CuS nanoprecipitates, bulk CuS, and the host material ZnS. The Si 111 monochromator was detuned 50% to reduce harmonics, and the slit height was 0.5 mm, providing an energy resolution ∼1.3 eV. A helium cryostat was used to collect the low temperature (4–300 K) data, and an oven was used for the higher temperatures (300–560 K).

For Cu EXAFS fluorescence measurements, the micro-encapsulated phosphor powder (ZnS:Cu,Cl, DuPont) was mixed with an organic binder and "blade wiped" onto either Scotch tape (cryostat measurements) or Kapton tape (oven measurements) in a ∼25 μm layer, and dried at 125 °C—these were referred to as 'as-made'. We also did some EXAFS studies on degraded test cells made with a 50 μm layer of powder, placed between an ITO coated substrate (mylar) and an evaporated Al layer; the ITO and Al served as electrodes (see figure 4(a) inset). For Zn in ZnS and Cu in CuS, the sample was first ground to less than 10 μm and then brushed onto tape; two tape layers encapsulate the powder. Two of these double layers were used for the EXAFS measurements.

3.2. EXAFS data reduction

The EXAFS data were reduced using standard techniques available in the RSXAP package [35] (see details in [36]). A pre-edge background was removed from the raw data and an experimental E_0 was defined as the energy of the half-height point on the K-edge. The post-edge background μ_0 was removed using four splines (five knots) for the Cu K-edge in ZnS:Cu; μ_0 approximates the background absorption in $\mu(E) = \mu_0(1 + \chi(E))$, where $\mu(E)$ is the Cu K-edge absorption coefficient and $\chi(E)$ is the EXAFS function. For the transmission scans, the Zn K-edge in ZnS:Cu,Cl and the Cu K-edge in CuS, six splines were used. The experimental function $\chi(E)$ was then transformed to k-space using the relation $k = \sqrt{\frac{2m(E-E_0)}{\hbar^2}}$. Examples of k-space data ($k\chi(k)$) at the Cu K-edge are shown for CuS reference at 4 K in figure 11(a) and for an as-made ZnS:Cu,Cl sample in figure 11(b). Next the k-space data k $\chi(k)$ were fast Fourier transformed (FFT) to r-space. Examples of the r-space data at several temperatures are shown in figure 12 for CuS, Cu K-edge data for as-made ZnS:Cu, and Zn K-edge data from ZnS:Cu. The first peak around 2 Å is the first neighbor Cu–S (or Zn–S) peak. Note that the positions of the EXAFS peaks do not reflect the real distances to the neighboring atoms about Cu (or Zn); the peak positions in the EXAFS plot are shifted to lower r. (For details, see [36], equation (1).)

The comparison of the three systems up to 300 K, presented in figure 12, shows that the first neighbor Cu–S (CuS or ZnS:Cu) and Zn–S peaks have similar temperature dependencies and therefore the Cu–S and Zn–S bonds are not greatly different in strength. The Zn–S peak has the weakest T-dependence and the Zn–S bond should therefore be the strongest. In contrast, much larger differences are found for the further neighbors. For the cubic ZnS structure, the second peak (3.5–4 Å) is mainly a Zn–Zn peak and at 300 K, it is not as strongly decreased as the second neighbor peaks for either of the Cu K-edge traces. Also at 300 K, the more distant neighbor peaks for CuS are very strongly damped. This is likely a consequence of the tetrahedral ZnS structure being more rigid than that of the layered CuS structure. The surprising result for the CuS-like precipitates in ZnS is that small peaks are observed beyond 6 Å and at 300 K, the further neighbor peaks are larger than for CuS. As pointed out earlier [9] for low T data, the presence of well defined peaks above 6 Å suggests

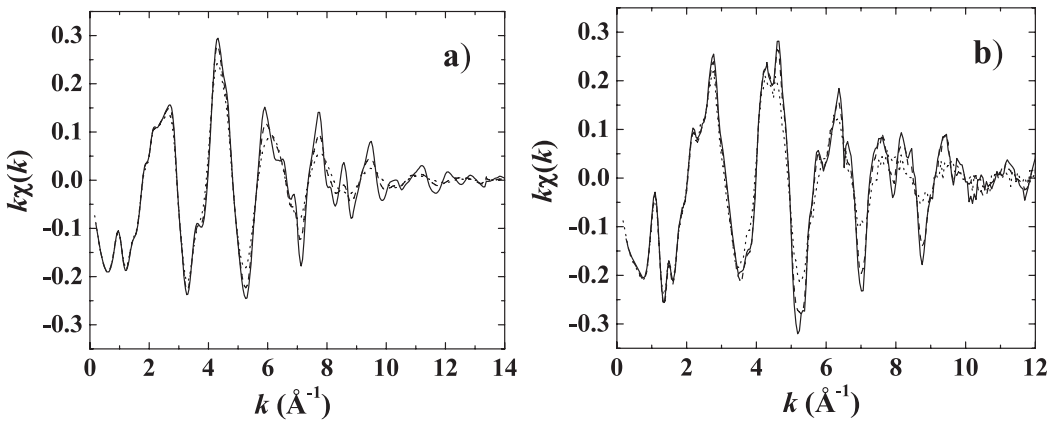

Figure 11. (a) Examples of k-space data for the high purity CuS reference sample at $T = 4$ (solid line), 140 (dashed line), and 300 K (dotted line); (b) examples of k-space data for the as-made ZnS:Cu,Cl sample at $T = 4$ (solid line), 100 (dashed line), and 300 K (dotted line).

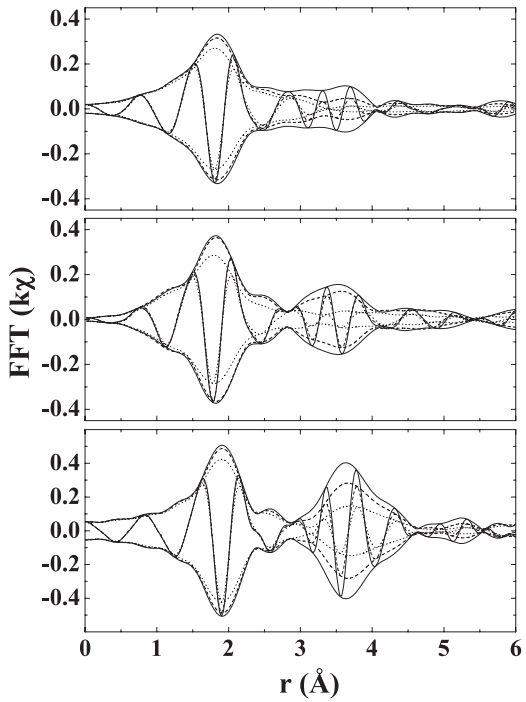

Figure 12. Fourier Transform of $k\chi(k)$ (r-space data) for top: high purity CuS at $T = 4$, 140 and 300 K, middle: the as-made ZnS:Cu,Cl sample, Cu K-edge, $T = 4$, 100, and 300 K and bottom: the Zn K-edge data for ZnS:Cu,Cl, $T = 4$, 140 and 300 K. The Fourier transform (FT) window is 3.5–11 Å^{-1} with a Gaussian broadening of width 0.3 Å^{-1}. In each plot the solid line is at 4 K, the dotted line is at 300 K, and the dashed line is for the middle temperature (100 or 140 K). In this and following r-space plots, the rapidly oscillating function is the real part, R, of the FT while the envelop function is $\pm\sqrt{R^2 + I^2}$ where I is the imaginary part of the FT.

that there is little or no amorphous layer about the precipitates and that the CuS precipitates are likely epitaxially connected to the ZnS host. Our comparison EXAFS study of degradation and thermal annealing effects (figure 13, 4 K) shows that there is negligible change in the local structure around the majority of Cu atoms, after either a 240 °C anneal or EL degradation—or a combination, EL degrade plus 240 °C anneal (not shown).

3.3. EXAFS data analysis

To parameterize the disorder (phonon and non-phonon) of the nearest neighbor Cu–S peak in ZnS:Cu, we need the Debye–Waller factor $\sigma^2(T)$, where σ is the width of the nearest neighbor pair distribution. We used the first peak in the 4 K spectra (Cu K-edge in ZnS:Cu,Cl) as an experimental standard and fit all the higher T data using this function to obtain the temperature dependence of $\sigma^2(T)$–σ^2(4 K) up to ∼550 K. Since the shape of the r-space peak changes with T particularly the shoulder between 2 and 2.5 Å, we shortened the fit range to 1.3–2.2 Å. For pure CuS and Zn K-edge in ZnS:Cu, we also used one of the 4 K data traces for that edge as the experimental standard and fit all the other traces to it to obtain $\sigma^2(T)$–σ^2(4 K) for these two bulk systems. These fits were carried out using rsfit [35]; the FT range for Cu in ZnS:Cu, was 3.5–11 Å^{-1}, while that for Zn K-edge and Cu K-edge in CuS was 3.5–14 Å^{-1}. Examples of the fits for the Cu–S peak are shown in figure 14.

In figure 15 we plot $\sigma^2(T)$–σ^2(4 K) for the nearest neighbor peak for CuS (Cu–S pair), ZnS:Cu (Cu–S pair), and ZnS:Cu (Zn–S pair). These plots provide a quantitative assessment of the strengths of the metal-S bonds in the three materials and confirm the qualitative results suggested in figure 12 up to 300 K. In addition, for the Cu K-edge in ZnS:Cu,Cl, $\sigma^2(T)$–σ^2(4 K) increases smoothly up to 550 K, and these data are well described over the entire temperature range using a correlated Debye model for phonons. There is no unusual change in the slope, or any step near or above 200 °C that would indicate some non-thermal-phonon change in the local distortions. This means there is no significant change of the CuS precipitates that might provide an explanation for the observed thermal degradation observed after a 240 °C anneal. Note however, that a small rearrangement of the precipitate structure, such as a rounding of the proposed needle-like tips, would not be observed because it would involve only a few per cent of the nanoprecipitate.

The correlated Debye temperatures for the three systems (first neighbor peak) are $\theta_{cD} = 431$ K for CuS, 392 K for Cu–S in ZnS:Cu, and 479 K for Zn–S in ZnS:Cu. Including systematics and small variations using different fit ranges etc,

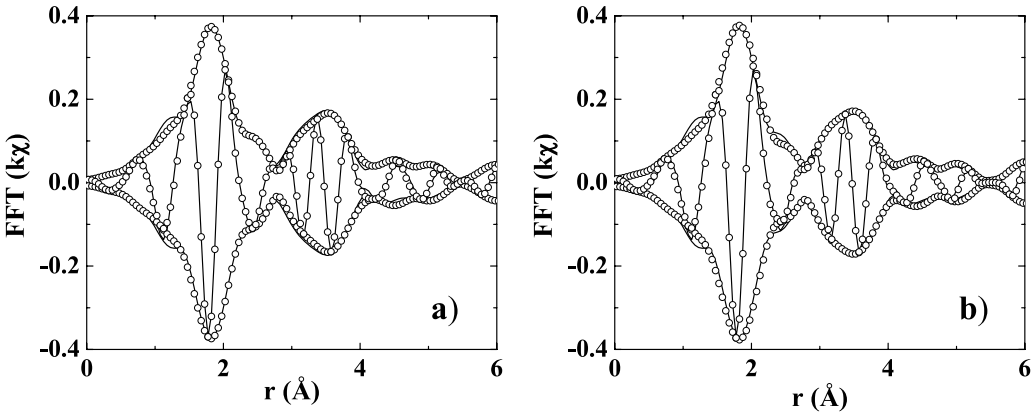

Figure 13. Comparison of EXAFS r-space data at 4 K for (a) as-made sample (solid lines) and after a 240 °C anneal (open circles), and (b) as-made device (solid lines) and after EL degradation (open circles). Both plots show that after a high T anneal or after EL degradation the environment around most of the Cu is unchanged.

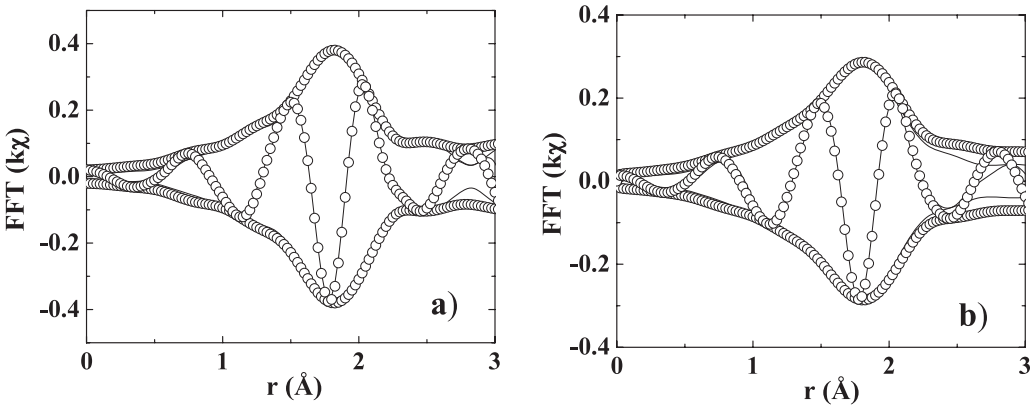

Figure 14. (a) An example of the fit of the Cu K-edge data for the as-made ZnS:Cu sample at 4 K; the fit range was 1.3–2.2 Å. (b) Data and fit for the as-made sample at 300 K; fit range 1.3–2.2 Å. The k-range for both fits is from 3.5 to 11.0 Å^{-1}. Data—solid line; fit—open circles. All of the high temperature data were fit using this shorter r-space fit range. Note different scales are used to plot the data.

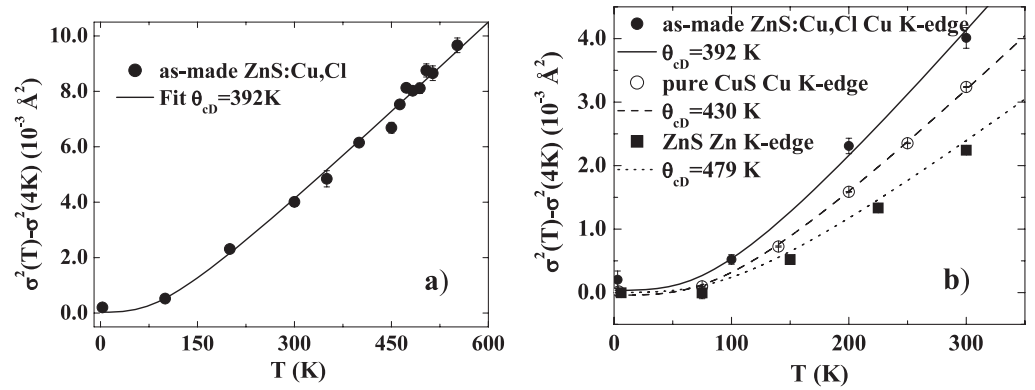

Figure 15. (a) Plot of $\sigma^2(T)$–σ^2(4 K) up to 550 K for the Cu–S pair in as-made ZnS:Cu,Cl and a fit to the correlated Debye model (solid line). Note that the same correlated Debye model fits both the low T and high T data, indicating no changes in local static distortions. (b) Comparison of $\sigma^2(T)$–σ^2(4 K) for the CuS pair in ZnS:Cu,Cl and CuS and the Zn–S pair in ZnS:Cu up to 300 K. Solid circles—Cu–S in ZnS:Cu data; open circles—Cu–S in CuS; solid squares—Zn–S in ZnS:Cu. The solid, dashed, and dotted lines are the corresponding correlated Debye fits to these data. The correlated Debye temperatures, θ_{cD}, are 392, 431, and 479 K respectively. Note that the relative error bar is comparable to the size of the symbols and the scatter in the data.

our estimation of the uncertainties in θ_{cD} are less than ±20 K for the bulk samples and ±20–30 K for fluorescence Cu data for ZnS:Cu.

One of the models proposed for the blue (Cu–B) emission center consists of two Cu^+ atoms, one substitutional on a Zn site and the other interstitial [10]. There are two interstitial

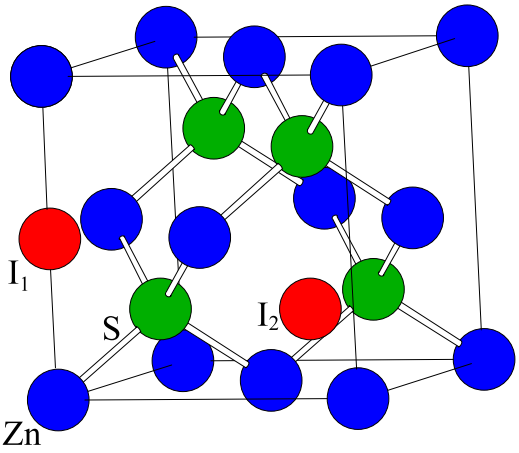

Figure 16. The two possible interstitial Cu sites in cubic ZnS lattice. The dark (blue) circles are Zn, and light (green) circles are S of the ZnS lattice. The shaded (red) circles are two interstitial Cu sites labeled I1 and I2. Due to symmetry, we only show one example for each site.

sites in the ZnS lattice as shown in figure 16. Site 1 (I1 in figure 16) has four S neighbors at the usual Zn–S distance but six Zn neighbors at a short distance—2.7 Å (about 2.4 Å on the EXAFS *r*-space plots). Site 2 (I2 in figure 16) has 4 closest Zn neighbors at the Zn–S distance. These positions are quite different from the various neighbor peaks for the ZnS structure or the CuS structure—for example the amplitude near 2.4 Å in the EXAFS data is small, and the phase for Zn–Zn is significantly different from Zn–S. Although much of the Cu is in the CuS precipitates, precipitation starts about 400–500 ppm. Thus for these samples with ∼1500 ppm, 25–30% of the Cu should be isolated centers and we can place an upper limit on the fraction of interstitial Cu from the EXAFS spectra. Before including the interstitial sites in the fits we first fit the data to a sum of 75% CuS and 25% Cu substitutional on Zn sites. The fit is not very sensitive to small decreases in the fraction of isolated Cu but this fraction cannot go much higher. Once these fits were obtained we added the possibility of interstitial site occupancy and modified the amplitudes accordingly; we also kept the parameters for the CuS fraction fixed.

Fits which include interstitial site peaks push the amplitude of these peaks close to zero. The Cu–Zn peaks have a large amplitude compared to the Cu–S peaks and we can determine the presence of interstitial Cu–Zn peaks down to a limit of order 3%. Thus at most a small fraction of the emission centers (∼10%) might involve interstitial Cu^+.

4. Discussion and conclusions

4.1. Spectral results, degradation and rejuvenation

The spectra shown in figures 7 and 10 are relatively complex and require a sum of four Gaussians to model the structure well as described in section 2.3. We first compare the emission peaks observed in the AC EL with the well-known photoluminescence (PL) peaks reported in the literature—see section 1.1. For PL, within the spectral range of interest here (400–600 nm), there are three blue peaks at very nearly the same energy (2.8 eV, ∼440 nm), all associated with complex hole centers, and a green peak (2.4 eV, ∼520 nm). The latter is believed to involve a simple hole trap, Cu^+ substituted on a Zn site, that does not have the reduced symmetry associated with more complex centers such as the blue centers. The dominant AC EL peak for 100 kHz operation occurs at 2.74 eV, very close to the 2.8 eV PL blue line, while at low AC frequency the dominant green line (2.44 eV) is also close to the PL green line. In terms of absolute values (see figure 5(a)), as the AC frequency increases the green peak near 2.4 eV increases slowly but only by a factor of 4–5 from 1 to 100 kHz. In contrast, the amplitude of the blue line near 2.8 eV increases dramatically, about a factor of 100, between 1 and 100 kHz. This suggests that even at 1 kHz the green line is close to saturation. There are no clear counterparts in PL to the middle two lines in the AC EL spectra at 2.61 and 2.67 eV, but note that they are only ∼ 0.2 eV away from one of the PL lines—a value comparable to the range of energy separations for the shallow electron traps [8, 15]. In addition, because the amplitude of line #2 is so small we will ignore it in the rest of the discussion.

Since the AC EL emission depends on the differences between the energies of the trapped electron and hole states, a simple way to understand this complex spectra is in terms of several distinct hole and electron trap states. However one of the very unusual features of the spectra during degradation is that the entire spectra maintains the *same* shape even after the emission is degraded down to 10–20%; it is only an overall magnitude change. Furthermore, this is observed for all AC frequencies, from operation at 100 kHz for which blue emission dominates, to low AC frequencies, ($\leqslant$1 kHz), at which green emission is largest. The shape also does not change after rejuvenation at 180 °C for 100 kHz operation and only changes slightly for 1 kHz operation.

These observations place severe constraints on the mechanisms for degradation/rejuvenation. First, to explain the shape change and the shift towards blue for higher AC frequency operation requires the presence of both deep and shallow traps, with the lifetime of the deeper traps longer than the shallow traps. For low frequency operation (weak electron–hole injection) mainly the deeper traps are occupied leading to primarily green emission. As electron–hole injection increases (with increasing AC frequency) the deepest traps become almost completely filled and the green emission (2.4 eV) starts to saturate. At this point slightly shallower traps become populated and a higher energy emission (2.66 eV) increases in amplitude. At still higher injection rates (10–100 kHz), this second trap state begins to saturate and a third, very shallow trap state becomes populated, leading to the blue emission at 2.74 eV. Note that in figure 10(b), the relative amplitude for line #3 (2.66 eV) first grows with increasing AC frequency and then clearly decreases above 5 kHz.

In the literature there are reports that a number of shallow electron trap sites exist over the range 0.1–0.8 eV below the conduction band [8, 15], Consequently, one possibility is that the shallow trap sites implied in our EL emission data are electron traps although we cannot directly

differentiate between holes and electrons. To keep the spectral shape constant during degradation requires that for a given AC frequency, the occupation ratios of the filled electron trap states must remain constant during degradation. In addition, the electron–hole recombination that produces the EL luminescence cannot be the rate-limiting factor in determining the populations of the different trap sites, as then when the EL emission is weak after degradation, the shallower trap sites would fill more easily.

Assuming the above set of shallow electron traps exist and that there is only one hole trap site, (substitutional Cu^+ on a Zn site) then if the number of filled hole trap states were reduced (e.g. via some diffusion mechanism), the overall EL emission would decrease with no shape change of the spectra. In fact, Hirabayashi *et al* [29] have previously argued that Cu diffusion under high E-fields is a likely explanation for the observed degradation. Thus the diffusion of Cu may well play a very important role in the rejuvenation/degradation processes;—several possibilities exist. If Cu^+ defects diffuse to the Cu_xS precipitates and thereby deplete the number of acceptor sites near a Cu_xS precipitate, that would degrade the EL emission. If the reverse is true during annealing at moderate temperatures—i.e. Cu atoms near the surface of the precipitate diffuse away from the precipitate, it would increase the number of acceptor sites and hence increase the EL emission. Chen *et al* [16] have recently proposed another mechanism—that diffusion under electric fields leads to a reduced conductivity of the Cu_xS precipitates which in turn decreases the enhancement of the local electric field and hence a reduction in the AC EL emission. However, a reduction in the E-fields by a reduction in the voltage would change the output color from blue to green at 100 kHz. We do not see any spectral change with degradation for our samples; thus this mechanism does not explain the EL degradation we observe, but might be involved in the thermal degradation.

If there are two (or more) hole trap states (e.g. for the blue [23, 10, 18, 26] and green [18, 15] emission centers observed in PL) the concentration ratio(s) of these hole traps would have to remain constant during degradation (all hole trap concentrations would have to decrease at the same rate) to retain the same spectral shape—a surprising requirement as different types of defects usually have quite different diffusion constants. Other alternatives include the possibility of having more complex centers with two or more excited states, such that the ratio of recombinations to each state remains constant.

The data in the literature are less clear about closely spaced hole trap sites but Apple and Prenner [25], using infrared spectroscopy report energy splittings of 0.74 and 0.95 eV for the Cu defects, and these may be modified by the presence of Cl^- at different distances from the Cu site. Thus one cannot exclude the possibility of a set of closely spaced hole trap states. Here the argument would be reversed—three hole trap states and one donor trap state would lead to the three main emission lines, with the green line the transition from the electron trap site to the deepest hole trap site. In this case diffusion of the electron trap site (usually assumed to be Cl^-) away from the precipitates would lead to reduced emission but maintain the same spectral shape, while a modest (rejuvenating) anneal could make the Cl defect distribution more uniform with some Cl diffusing back towards the CuS precipitates. Support for a Cl^- diffusion model comes from Jaffe [32] who suggests that Cl^- diffuses away and leaves a S vacancy behind. In addition Jaffe reported that for their best ZnS:Cu,Cl and ZnS:Cu,Br phosphors, the Br co-activator compounds had significantly longer half-lives for degradation—by at least a factor of 5.

The only other report of a rejuvenation effect was for a similar system with Br as the co-activator instead of Cl [17]. Unlike the results presented here in which most of the rejuvenation occurs in 30 min, the rejuvenation in the ZnS:Cu,Br system occurs very slowly for temperatures 157–185 °C—over a time of order 10 h. Although there is no way to compare other aspects of the two materials the strong difference between a Br and Cl co-activator is suggestive of a Cl/Br diffusion mechanism, as the heavier Br would diffuse more slowly. More experiments are needed to probe this difference under more identical conditions.

Another degradation model was developed by Fischer [14, 8] who suggested in the 1960s that there might be a reduced efficiency in electron–hole injection from the CuS precipitates as a result of blunting of the tips on the precipitates. Assuming an induced charge q on a needle-like CuS precipitate, the E-field around a tip $\sim q/R^2$ and the enhancement of the field is $\sim(L/R_T)^2$ where L is the length of the needle and R_T is the tip radius [13, 8]. The field is a maximum at the tip and decreases away from the tip, with field injection determined by the high field at the tip surface. If the radius becomes larger from blunted tips, then one would expect reduced electron–hole injection [8] and hence a change in the shape of the spectra as the material degraded; i.e. a decreased injection efficiency should be similar to a decrease in AC frequency. We suggested above that the blue emission occurs when the device is driven fast enough that the deepest trap sites become completely filled and several shallower trap sites are then partially filled; however, if the ejection efficiency were significantly reduced during degradation via Fischer's model, the deeper trap sites would not be completely filled and the spectra would shift less and have a stronger green component, which is not observed. Thus a reduced injection efficiency as a result of damage to the CuS needle tips cannot be the main mechanism for degradation, unless some other explanation for the shape change with AC frequency can be found. Note also that Hirabayashi *et al* have reported that up to '83, no convincing evidence had yet been found for Fischer's mechanism [29].

The situation is quite different for the 240 °C annealed samples; in this case, all spectra are shifted towards the green. This would be consistent with a reduced electron–hole injection efficiency as a result of degraded tips on the precipitates. For these samples, if it is not the injection efficiency that is reduced in the anneal, then the number of deep electron traps would have to increase such that the deep levels are not filled as quickly. Since there is no obvious reason why the number of deep traps should be concentrated via diffusion, we propose that degradation of the precipitate tips is a viable mechanism for the thermally induced degradation, or possibly the model suggested by Chen *et al* [16], in which

the conductivity of the precipitates decreases. Since Cu is a fast diffuser [8] and the Cu diffusion constant increases [37] with T, a rearrangement of the Cu atoms near the tip during annealing or within the CuS nanoprecipitate is plausible.

Yet another possibility was proposed by Roberts [38] who suggested that nearest neighbor Cu^+–Cl^- pairs may be inactive in AC EL and hence that the formation of such pairs would lead to decreased EL emission. He associated Cl^- with the deepest electron traps—and in that case, formation of Cu–Cl pairs would remove some of the hole trap sites and one type electron trap site. This would be inconsistent with the constant shape of the spectra observed during degradation in measurements. However if the Cl^- were associated with a very shallow electron trap level, we could not eliminate this model.

The new data, plus the previous results reviewed above indicate that the most likely explanations for EL degradation in ZnS:Cu,Cl are that both Cu and Cl (Br) are diffusing towards or away from the precipitates in the bulk material when high electric fields are present. Unfortunately a more definitive model is not yet possible.

Finally, the rejuvenation experiments plus the results for a sample annealed at 240 °C before preparing EL test cells, indicate that at least two mechanisms are at play during thermal annealing. For moderate temperature anneals, 130–180 °C, the AC EL intensity recovers very rapidly with time suggesting a rapid diffusion process (figure 9 inset) but full rejuvenation is not achieved. For this material at 100 kHz, the rejuvenated emission achieved via an anneal near 180 °C increases to about 72%, after degradation to about 20%. Although significant, it is less than the ∼90% we observed earlier [9] with a different binder. We have repeated the present experiment several times and the rejuvenation is generally between 70 and 75% for this batch of phosphor and binder. We have no clear explanation for the larger rejuvenation observed earlier, but expect that it is likely phosphor dependent.

The ability to rejuvenate the sample several times in successive anneals is also consistent with a diffusive process in which the distribution of centers is randomized via diffusion. However the change in shape of the rejuvenated spectra at 1 kHz for a 180 °C anneal (figure 5), the decrease in rejuvenated EL intensity with time when the annealing at 200 °C extends beyond one hour (figure 9 inset) and the strong EL degradation and change in spectral shape when the powder is annealed at 240 °C figure 6, all indicate that another mechanism is needed at elevated temperatures which we have proposed is caused by a reduced electron–hole injection efficiency as a result of rounding of the CuS precipitates. However we first needed to verify that most of the CuS-like precipitates remained after the anneal as described in the next section. Now that we recognize that two mechanisms are likely present above 180 °C, future experiments are planned at lower T for longer times to see if a larger rejuvenation is possible.

4.2. EXAFS, local structure, and CuS

Based on the increased degradation and spectral change, observed after ZnS:Cu,Cl material was annealed (from 200 to 240 °C), further EXAFS studies were carried out to look for structural changes at elevated temperatures and also to more carefully compare the Cu environment in ZnS:Cu,Cl with that in bulk CuS. In this set of experiments, nothing unusual was found. $\sigma^2(T)$–$\sigma^2(4\ \mathrm{K})$ varied smoothly from 4 to 550 K (see figure 15(a)), consistent with the correlated Debye model, and no changes in slope or steps in $\sigma^2(T)$ were observed. Also, no significant change in the Cu–S distance was observed. Further the low T EXAFS data show the same local structure as obtained for the as-made material—no significant loss/change of the CuS precipitates takes place. Thus the CuS precipitates remain relatively unchanged although minor changes such as the possible rounding of sharp tips on the precipitates, would not be observed.

Finally we searched for evidence of any Cu^+ interstitial sites [10] which have been proposed for one of the blue emission center but did not find any. We place an upper level that at most 10% of the emission sites involving Cu might be interstitial sites. Our data are consistent with no interstitial sites. Samples with much lower Cu concentrations are needed to check this more carefully and are planned for the future.

4.3. Summary

The major results from this investigation are:

(1) Under AC EL degradation, the shape of the spectra does not change for a given AC excitation; that puts severe constraints on possible degradation mechanisms; in particular it is inconsistent with Fischer's proposal that sharp tips on the precipitates become rounded.
(2) The EL emission spectra are primarily the sum of three peaks (plus a weak but sharp peak) and each spectra (one for each AC excitation frequencies) can be fit using the same peak widths and positions; only the amplitudes vary with excitation frequency.
(3) Test cells can be degraded and rejuvenated several times, but each time the rejuvenated emission becomes smaller. The optimum temperature for rejuvenation is about 180 °C.
(4) For moderate temperature anneals from 200 to 240 °C, the shape of the emission spectra has an increasing red-shift for a fixed excitation frequency. This indicates another mechanism must be operative.
(5) The EXAFS experiments show that at elevated temperatures there are no significant changes in the CuS-like precipitates—they do not break-up into smaller nanoparticles or dissociate and diffuse into the host lattice.
(6) EXAFS experiments at low T also provide no evidence for interstitial Cu, needed for one of the proposed Cu pair centers—the experiments are consistent with no interstitial Cu, but the upper limit is that <10% of the isolated Cu might be interstitial.

Acknowledgments

The work at UCSC was supported by DOE grant DE-FG02-07ER46388. We thank M. Kozina for characterizing some of the materials, J Zhang, C Corrado and Chris France for

helpful discussions. The EXAFS experiments were performed at SSRL (operated by the DOE, Division of Chemical Sciences, and by the NIH, Biomedical Resource Technology Program, Division of Research Resources).

References

[1] Shionoya S 1999 *Phosphor Handbook* ed S Shionoya and W M Yen (New York: CRC Press) chapter 3, pp 231–58
[2] Tanaka S, Kobayashi H and Sasakura H 1999 *Phosphor Handbook* ed S Shionoya and W Yen (New York: CRC Press) chapter 9, pp 601–12
[3] Sidot M 1866 *C.R. Acad. Sci.* **62** 999
[4] Destriau G 1936 *J. Chim. Phys.* **33** 620
[5] Pattrick R A D, Mosselmans J F W and Charnock J M 1998 *Eur. J. Mineral.* **10** 239
[6] Withnall R, Silver J, Ireland T G, Fern G R and Marsh P J 2009 *J. Electrochem. Soc.* **156** J326
[7] Gillson J J L and Darnell F J 1962 *Phys. Rev.* **125** 149
[8] Fischer A G 1963 *J. Electrochem. Soc.* **110** 733
[9] Warkentin M, Bridges F, Carter S A and Anderson M 2007 *Phys. Rev.* B **75** 075301
[10] Blicks H, Riehl N and Sizmann R 1961 *Z. Phys.* **163** 594
[11] Bol A A, Ferwerda J, Bergwerff J A and Meijerink A 2002 *J. Lumin.* **99** 325
[12] Destriau G and Ivey H F 1955 *Proc. IRE* **43** 1911
[13] Maeda K 1960 *J. Phys. Soc. Japan* **15** 2051
[14] Fischer A G 1962 *J. Electrochem. Soc.* **109** 1043
[15] Suzuki A and Shionoya S 1971 *J. Phys. Soc. Japan* **31** 1455
[16] Chen F, Kitai A H and Xiang Y 2009 *J. Electrochem. Soc.* **156** H585
[17] Hirabayashi K and Itoh Y 1982 *J. Electrochem. Soc.* **129** 362
[18] Shionoya S, Koda T, Era K and Fujiwara H 1964 *J. Phys. Soc. Japan* **19** 1157
[19] Kröger F A 1940 *Physica* **7** 1
[20] Prener J S and Williams F E 1956 *J. Chem. Phys.* **25** 361
[21] Kasai P H and Otomo Y 1962 *J. Chem. Phys.* **37** 1263
[22] Shionoya S, Urabe K, Koda T, Era K and Fujiwara H 1966 *J. Phys. Chem. Solids* **27** 865
[23] Bowers R and Melamed N T 1955 *Phys. Rev.* **99** 1781
[24] Holton W C, de Wit M, Watts R K, Estle T L and Schneider J 1969 *J. Phys. Chem. Solids* **30** 963
[25] Apple E F and Prener J S 1960 *J. Phys. Chem. Solids* **13** 81
[26] Urabi K, Shionoya S and Suzuki A 1968 *J. Phys. Soc. Japan* **25** 1611
[27] Thornton W A 1956 *Phys. Rev.* **102** 38
[28] Kasai P H and Otomo Y 1961 *Phys. Rev. Lett.* **7** 17
[29] Hirabayashi K, Kozawaguchi H and Tsujiyama B 1983 *J. Electrochem. Soc.* **130** 2259
[30] Thornton W A 1960 *J. Electrochem. Soc.* **107** 895
[31] Lehmann W 1966 *J. Electrochem. Soc.* **113** 40
[32] Jaffe P M 1961 *J. Electrochem. Soc.* **108** 711
[33] Ibanez J, Garcia E, Gil L, Mollar M and Mari B 2007 *Displays* **28** 112
[34] Nien Y-T and Chen I-G 2006 *Appl. Phys. Lett.* **89** 261906
[35] See http://lise.lbl.gov/RSPAK
[36] Jiang Y, Bridges F, Downward L and Neumeier J J 2007 *Phys. Rev.* B **76** 224428
[37] Bacaksiz E, Dzhafarov T D, Novruzov V D, Ozturk K, Tomakin M, Kucukomeroglu T, Altunbas M, Yanmax E and Abay B 2004 *Phys. Status Solidi* a **201** 2948
[38] Roberts S 1957 *J. Appl. Phys.* **28** 262